Thickness dependence of electronic phase transitions in epitaxial V_2O_3 films on (0001) $LiTaO_3$

B. S. Allimi, M. Aindow, and S. P. Alpay[a)]
Materials Science and Engineering Program, Department of Chemical, Materials, and Biomolecular Engineering and Institute of Materials Science, University of Connecticut, Storrs, Connecticut 06279, USA

(Received 29 July 2008; accepted 18 August 2008; published online 18 September 2008)

Single crystal epitaxial thin films of V_2O_3 were grown on (0001) $LiTaO_3$ by pulsed laser deposition. X-ray diffraction and atomic force microscopy data show that the deposits were initially pseudomorphic, that they underwent plastic relaxation at a critical thickness of ≈16 nm, and that relaxation is accompanied by the development of surface roughness, increasing with deposit thickness. These effects lead to changes in electrical properties of the films as a function of temperature. As film thickness increases the properties go from insulator-insulator to metal-insulator, then metal-metal transitions. The thickest films (>200 nm) remained metallic over the temperature range of the measurements. © *2008 American Institute of Physics*.
[DOI: 10.1063/1.2978352]

Vanadium sesquioxide (V_2O_3) typifies material systems exhibiting a metal-to-insulator transition (MIT) as a function of temperature, pressure, and doping concentration.[1] At an ambient pressure of 1 atm, V_2O_3 transforms from a rhombohedral paramagnetic metal to a monoclinic antiferromagnetic insulator phase upon cooling to 160 K, with a jump in the resistivity of about seven orders of magnitude.[2] This behavior has stimulated extensive theoretical and experimental research on V_2O_3.[3–7] Various methods have been devised to grow high-quality V_2O_3 thin films, both for samples to study the physics of the MIT in thin films and as the basis for potential sensing and actuation devices.[8–11] While such films can be produced using pulsed laser deposition (PLD), this is usually done using a V_2O_5 target while exerting careful control of deposition conditions to give V_2O_3 deposits.[7] In a recent paper we have reported the synthesis of high-quality epitaxial V_2O_3 films on $\{11\bar{2}0\}$ and (0001) sapphire (α-Al_2O_3) substrates via PLD using a powder-pressed pure V_2O_3 target in an evacuated deposition chamber.[12] The films on (0001) α-Al_2O_3 displayed a MIT at $T=180$ K compared to $T=160$ K in single-crystal V_2O_3. The films on $\{11\bar{2}0\}$ α-Al_2O_3, however, showed an insulator-to-insulator transition at $T=186$ K. For films on (0001) α-Al_2O_3 the in-plane and out-of-plane strains were determined via x-ray diffraction (XRD) to be $\varepsilon_1=\varepsilon_2=-0.22\%$ and $\varepsilon_3=-0.13\%$, respectively. In films on $\{11\bar{2}0\}$ α-Al_2O_3, there existed an anisotropic in-plane strain state with $\varepsilon_1=1.20\%$ and $\varepsilon_2=-1.15\%$. The variations in the phase transformation characteristics and in the resistivities of these films were thus attributed to different levels of strain and commensurate changes in the film morphologies.[13] In this letter, we present a study on the role of film thickness and internal strain on the electrical properties of V_2O_3 thin films deposited by PLD from V_2O_3 targets onto (0001) $LiTaO_3$ substrates. Such substrates have been used previously for the epitaxial deposition of V_2O_3,[7] and the magnitude of the isotropic in-plane misfit (3.9%) is similar to that for growth on (0001) α-Al_2O_3 (−4.1%), although this is of the opposite sign.

V_2O_3 thin films were deposited onto (0001) $LiTaO_3$ substrates using a KrF pulsed excimer laser with a wavelength of 248 nm, an energy of 240 mJ/pulse, a pulse length of 20 ns, and a repetition rate of 6 Hz. The laser was focused on a powder-pressed stoichiometric V_2O_3 target rotating at 35 rpm. The laser fluence was estimated at about 2.8 J/cm^2, and this gave a growth rate of about 0.08 – 0.16 nm/s. The substrates were rotated at 20 rpm during deposition to promote homogenous growth of the films. The details of the fabrication of the target and of the deposition parameters have been presented elsewhere.[12] Portions of the substrate were masked to enable the thickness of the film h to be measured using atomic force microscopy (AFM) at the edge of the masked region. Films with $h=12-406$ nm were grown in this study.

A general area detector diffraction system diffractometer was used to collect XRD patterns from each of the films, and these patterns confirmed that the deposits were single-crystal epitaxial films. The conventional XRD spectra obtained from the films with $h=12$, 87, 200, 370, and 406 nm are shown in Fig. 1. These $\theta-2\theta$ scans were collected with the source and detector inclined equally to the substrate surface normal. As expected, the spectra contain only (000l) peaks from the substrate and deposit, except for the 370 nm film whose spec-

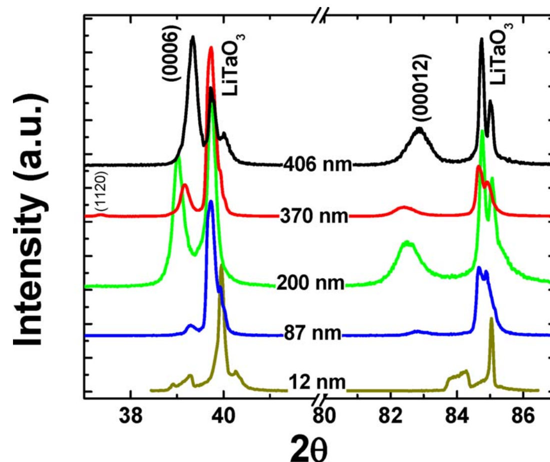

FIG. 1. (Color online) XRD patterns of V_2O_3 thin films on c-$LiTaO_3$ substrates of different thicknesses ranging from 12 to 406 nm.

[a)]Author to whom correspondence should be addressed. Electronic mail: p.alpay@ims.uconn.edu.

 © 2008 American Institute of Physics

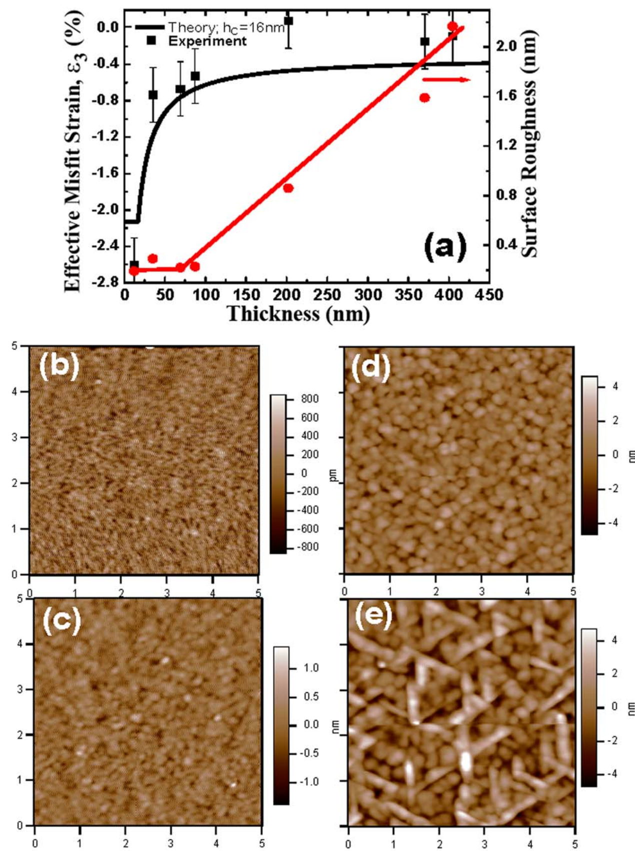

FIG. 2. (Color online) (a) Out-of-plane strain in the V_2O_3 film as a function of the film thickness (solid squares). The solid line represents the theoretical effective out-of-plane misfit strain of V_2O_3 films on *c*-$LiTaO_3$ as a function of thickness computed at critical thickness of 16 nm from MB criteria. Also plotted is the rms surface roughness (solid circles). AFM images displaying the surface morphology are shown in (b) 12 nm, (c) 87 nm, (d) 202 nm, and (e) 370 nm thick films. The scan area is 5×5 μm^2.

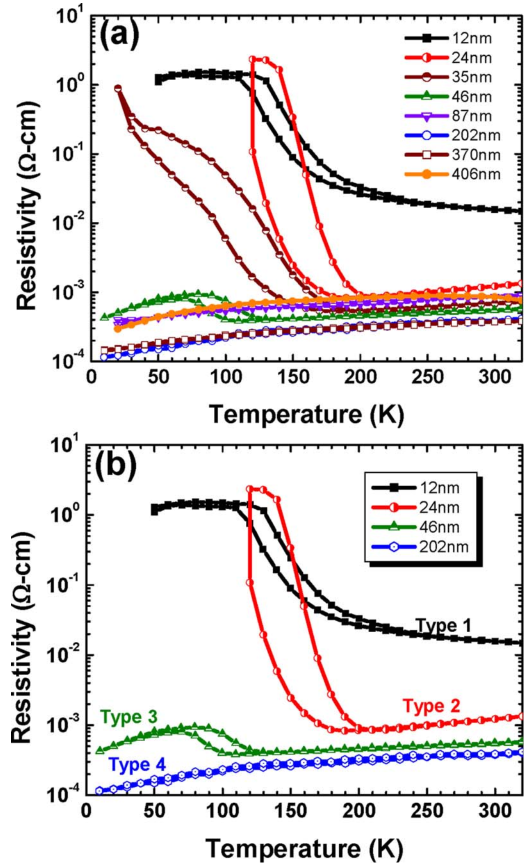

FIG. 3. (Color online) (a) Temperature dependence of the resistivity of V_2O_3 thin films on *c*-$LiTaO_3$ substrates for $h=12$, 24, 35, 46, 87, 202, 370, and 406 nm. (b) Four different behaviors were observed and these are $h=12$ nm (IIT, type 1), $h=24$ nm (MIT, type 2), $h=46$ nm (MMT, type 3), and only *M* for $h=202$ nm.

trum also displays a $\{11\bar{2}0\}$ V_2O_3 peak. The out-of-plane component of the strain in the film ε_3 was obtained from such data using the substrate peaks as a reference.

The values of ε_3 obtained by XRD are plotted in Fig. 2 and these vary from $\varepsilon_3=-2.6\%$ for $h=12$ nm to $\varepsilon_3\approx0$ for $h\geq200$ nm. This indicates that the film is initially pseudomorphic and that plastic relaxation occurs beyond a critical value of h, h_c. In the absence of any data on the misfit accommodation mechanism, we have estimated h_c using the original analysis of Matthews and Blakeslee (MB).[14] Substituting bulk values for the lattice parameters, 0.33 for Poisson's ratio and $\frac{1}{3}[11\bar{2}3]$ for the Burgers vector, the MB analysis gives $h_c=16$ nm. Following Speck and Pompe[15] and Alpay *et al.*,[16] this value has been used to calculate the variation in ε_3 expected with increasing deposit thickness as misfit dislocations are introduced, this is indicated by the bold line in Fig. 2(a). This line matches the experimental data very well when one considers the possible experimental errors and the assumptions involved in the calculation.

The surface morphologies of the films were evaluated using AFM and in all cases the rms surface roughness R was <2.5 nm. Four examples of AFM images are shown in Figs. 2(b)–2(e). All of the images showed self-similar morphologies with the exception of the 370 nm film, which exhibited a secondary surface deposit. These deposits appeared as three sets of laths, 1 μm long by 0.2 μm across lying parallel to $\langle 11\bar{2}0\rangle$ in the surface: the $\{11\bar{2}0\}$ peak in the XRD spectrum from this film presumably arises from these laths. The values of R are plotted against h in Fig. 2(a) and it is clear that the roughness only starts to increase after the onset of plastic relaxation, whereupon R increases linearly with h. The development of surface roughness with deposit thickness as a secondary relaxation mechanism after misfit dislocation introduction has been well documented for epitaxial semiconductors[17,18] and it seems likely that the roughening observed here occurs by similar processes.

Electrical resistance measurements were performed using a Displex system equipped with a LAKESHORE temperature controller software package. The Van de Pauw and standard four-point probe methods were used to measure the in-plane transport properties of all the films as a function of temperature over the range 10–340 K. Figure 3(a) is a plot of the temperature dependence of resistivity for each of the films. Four different types of electrical transitions were observed, as highlighted in Fig. 3(b). Such transitions have been reported previously in V_2O_3 films on other substrates,[5,13,19,20] but we observe here all four types of transitions in the same film-substrate system.

The thinnest film ($h=12$ nm) displays an insulator-insulator transition (IIT) (type 1), where the resistivity increases with decreasing temperature down to $\sim$220 K followed by a jump of approximately two orders of magnitude. Films with $h=24$ and 35 nm exhibit the expected MIT (type 2). There is a decrease in the resistivity with decreasing

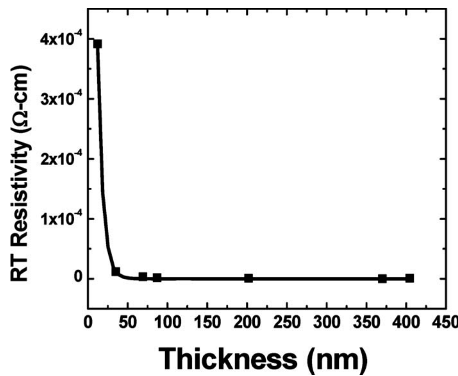

FIG. 4. Room temperature resistivity of the V_2O_3 films as a function of film thickness.

temperature down to ~190 K followed by a jump of approximately three orders of magnitude. We note that this transition occurs at a temperature ~30 K higher than bulk V_2O_3 and the change in the resistivity at the phase transformation is four orders of magnitude smaller. The 46 nm sample shows a metal-metal transition (MMT) (type 3), where there is a linear decrease in resistivity with decreasing temperature down to $T \approx 128$ K followed by a small jump in resistivity. For temperatures lower than 72 K, the sample displays typical metallic behavior with a decrease in the resistivity as the temperature is lowered further. Thicker films ($h > 80$ nm) demonstrated only metallic (M) (type 4) behavior over the whole temperature range with no indication of a phase transformation.

One of the interesting aspects of the data shown in Fig. 3(a) is that the insulating phases in V_2O_3 are systematically eliminated with increasing film thickness. The high temperature insulating phase observed in the thinnest film ($h=12$ nm), which displays the IIT behavior, disappears as h is increased, resulting in an MIT in the films with $h=24$ and 34 nm. The low temperature insulating phase observed in 12, 24, and 34 nm thick films vanishes with further increases in h, leading to the emergence of a MMT in the 46 nm thick film. In films with $h=87-406$ nm, we see that a metallic phase is stabilized and the resistivity of the films decreases linearly as a function of temperature down to the temperature limit of our measurement system (10 K). The observed behavior follows a systematic order that can be summarized as IIT→MIT→MMT→M with increasing h. The plot of the room temperature (RT=25 °C) resistivity as a function of h is shown in Fig. 4. The resistivity values of the films decrease with increasing h, further demonstrating the stabilization of a metallic phase.

The IIT in the thinnest film is most likely due to the high in-plane tensile stresses. The compressive out-of-plane strain [Fig. 2(a)] calculated from the XRD data (Fig. 1) is consistent with a pseudomorphic film in biaxial tensile tension parallel to the substrate surface. As such, the in-plane interionic distances will be larger, leading to a separation of the a_{1g} and $e_g(\pi)$ bands and hence the insulating behavior above the phase transformation temperature. The overlap of these bands in bulk V_2O_3 results in metallic behavior above the MIT. After the onset of strain relaxation at $h \approx 15-20$ nm as confirmed by XRD, the in-plane tensile strains are greatly reduced and the expected MIT transition is observed in the 24 and 34 thick films. However, the absence of a phase transformation and the stabilization of the metallic phase in thicker films is a very surprising finding. Shifts in the MIT temperature and stabilization of the metallic phase have been observed in other PLD-deposited V_2O_3 films.[19,21] One would expect that with an increase in h and a commensurate relaxation of the epitaxial stresses, the thicker films would assume the properties of the bulk. Previous reports show that completely relaxed V_2O_3 films on (0001) α-Al_2O_3 tend to display the typical MIT of bulk V_2O_3.[5,13] We note that all electronic phase transformations in bulk V_2O_3 can be suppressed by the application of a hydrostatic pressure of about 23 kbar or by doping with Ti [for $(V_{1-x}Ti_x)_2O_3$ with $x > 0.05$, the antiferromagnetic insulator phase is completely suppressed].[22] Defects have highly localized short-range stress fields. In films with a dense misfit dislocation substructure and surface undulations, one could imagine that these stress fields would overlap, creating very thin "layers" at the film-substrate interface and at the surface with a different strain state than the rest of the film. The observed behavior in the thicker films might thus be related to specific defect microstructures that generate localized conditions equivalent to the application of a hydrostatic pressure in bulk. We are currently conducting a detailed microstructural analysis of the V_2O_3 films on both (0001) $LiTaO_3$ and (0001) α-Al_2O_3 in an attempt to identify the differences in defect structure that might lead to the contrasting electronic behavior.

This work was supported by the U.S. Army Research Office through Grant No. W911NF-05-1-0528. We also would like to thank D. M. Pease, J. I. Budnick, B. O. Wells, and C. Xie for many useful discussions.

[1] D. B. McWhan and J. P. Remeika, Phys. Rev. B 2, 3734 (1970).
[2] P. D. Dernier and M. Marezio, Phys. Rev. B 2, 3771 (1970).
[3] J. H. Park, L. H. Tjeng, A. Tanaka, J. W. Allen, C. T. Chen, P. Metcalf, J. M. Honig, F. M. F. de Groot, and G. A. Sawatzky, Phys. Rev. B 61, 11506 (2000).
[4] B. Sass, C. Tusche, W. Felsch, N. Quaas, A. Weismann, and M. Wenderoth, J. Phys.: Condens. Matter 16, 77 (2004).
[5] H. Schuler, S. Klimm, G. Weissmann, C. Renner, and S. Horn, Thin Solid Films 299, 119 (1997).
[6] I. Yamaguchi, T. Manabe, T. Kumagai, W. Kondo, and S. Mizuta, Thin Solid Films 366, 294 (2000).
[7] S. Yonezawa, Y. Muraoka, Y. Ueda, and Z. Hiroi, Solid State Commun. 129, 245 (2004).
[8] E. Andrich, Philips Tech. Rev. 30, 170 (1969).
[9] D. M. Moffatt, J. P. Runt, A. Halliyal, and R. E. Newnham, J. Mater. Sci. 24, 609 (1989).
[10] D. P. Partlow, S. R. Gurkovich, K. C. Radford, and L. J. Denes, J. Appl. Phys. 70, 443 (1991).
[11] R. S. Perkins, A. Ruegg, M. Fischer, P. Streit, and A. Menth, IEEE Trans. Compon., Hybrids, Manuf. Technol. 5, 225 (1982).
[12] B. S. Allimi, S. P. Alpay, D. Goberman, T. Huang, J. I. Budnick, D. M. Pease, and A. I. Frenkel, J. Mater. Res. 22, 2825 (2007).
[13] B. S. Allimi, S. P. Alpay, C. K. Xie, B. O. Wells, J. I. Budnick, and D. M. Pease, Appl. Phys. Lett. 92, 202105 (2008).
[14] J. W. Matthews and A. E. Blakeslee, J. Cryst. Growth 27, 118 (1974).
[15] J. S. Speck and W. Pompe, J. Appl. Phys. 76, 466 (1994).
[16] S. P. Alpay, V. Nagarajan, L. A. Bendersky, M. D. Vaudin, S. Aggarwal, R. Ramesh, and A. L. Roytburd, J. Appl. Phys. 85, 3271 (1999).
[17] R. Beanland, M. Aindow, T. B. Joyce, P. Kidd, M. Laurenco, and P. J. Goodhew, J. Cryst. Growth 149, 1 (1995).
[18] A. G. Cullis, D. J. Robbins, S. J. Barnett, and A. J. Pidduck, J. Vac. Sci. Technol. A 12, 1924 (1994).
[19] C. Grygiel, C. Simon, B. Mercy, W. Prellier, R. Fresard, and P. Limelette, Appl. Phys. Lett. 91, 262103 (2007).
[20] Q. Luo, Q. L. Guo, and E. G. Wang, Appl. Phys. Lett. 84, 2337 (2004).
[21] S. Autier-Laurent, B. Mercey, D. Chippaux, P. Limelette, and C. Simon, Phys. Rev. B 74, 195109 (2006).
[22] D. B. McWhan, J. P. Remeika, T. M. Rice, W. F. Brinkman, J. P. Maita, and A. Menth, Phys. Rev. Lett. 27, 941 (1971).